

## Raman and reflectivity spectra of cubic $\text{Cd}_{1-x}\text{Mn}_x\text{Se}$ epilayers grown by molecular-beam epitaxy

R. G. Alonso, Y. R. Lee,\* Eunsoon Oh, and A. K. Ramdas

*Department of Physics, Purdue University, West Lafayette, Indiana 47907-1301*

H. Luo, N. Samarth, and J. K. Furdyna

*Department of Physics, University of Notre Dame, Notre Dame, Indiana 46556*

H. Pascher

*Experimentalphysik I, Universität Bayreuth, D-8580 Bayreuth, Germany*

(Received 1 November 1990)

We present a Raman-scattering, reflectivity, and photoluminescence study of  $\text{Cd}_{1-x}\text{Mn}_x\text{Se}$  epilayers grown by molecular-beam epitaxy on (001) GaAs substrates. These epilayers exhibit the cubic (zinc-blende) structure, even though in bulk crystal growth this alloy crystallizes in the wurtzite form. The energy gap as a function of  $x$  is studied by reflectivity and photoluminescence. We also present a Raman study of the frequency of the zone-center optical phonons as a function of  $x$ , extending the previous work to higher values of  $x$ . The magnetic-field dependence of the spin-flip Raman shift of donor-bound electrons and of the free-excitonic photoluminescence shows the huge Zeeman shifts typically encountered in diluted magnetic semiconductors, allowing an estimate of the ratio between the conduction ( $\alpha$ ) and valence ( $\beta$ ) -band exchange constants,  $|\alpha/\beta|_{\text{cubic}}=0.80$ , a value somewhat larger than that in the wurtzite structure. We also investigate the Raman features associated with spin flip of donor-bound electrons in epilayers with large  $x$ , where the strong antiferromagnetic coupling comes into play. In addition, we report the anomalous behavior of photoluminescence peaks observed for high values of  $x$ , which we have attributed to deep impurity levels resulting in transition energies just above the 2.2-eV emission of  $\text{Mn}^{2+}$ .

### I. INTRODUCTION

The tetrahedrally coordinated II-VI diluted magnetic semiconductors (DMS's) have been thoroughly studied in the bulk, in either the zinc-blende or the wurtzite structure.<sup>1</sup> Earlier work on DMS's includes magnetic phenomena such as giant Faraday rotation<sup>2</sup> and spin-flip Raman scattering associated with donor-bound electrons,<sup>3</sup> where the large magnetic effects originate from the large spin-spin exchange between the  $d$  electrons of  $\text{Mn}^{2+}$  and the  $s$  electrons of the conduction band and the  $p$  electrons of the valence band (the so-called " $sp$ - $d$  exchange"). The Raman electronic paramagnetic resonance (Raman EPR) of  $\text{Mn}^{2+}$  observed in DMS's focuses on the ground-state Zeeman multiplet of  $\text{Mn}^{2+}$ , whereas its resonance enhancement for incident photon energies close to that of the excitonic transitions once again illustrates the unique role played by the  $sp$ - $d$  exchange interaction in these materials.<sup>3</sup> The antiferromagnetic coupling between the magnetic ions is demonstrated by the observation of (a) the Raman spectrum of  $\text{Mn}^{2+}$  pairs,<sup>4</sup> (b) the magnon feature<sup>5</sup> [Raman antiferromagnetic resonance (AFMR)], and (c) the evolution of the Raman EPR line into the high-frequency component of Raman AFMR in an external magnetic field.<sup>6</sup>

In a previous paper<sup>7</sup> on cubic  $\text{Cd}_{1-x}\text{Mn}_x\text{Se}$  and  $\text{Cd}_{1-x}\text{Zn}_x\text{Se}$ , grown on (001) GaAs substrates by molecular-beam epitaxy (MBE),<sup>8,9</sup> we confirmed, on the basis of our Raman-scattering study, the cubic (zinc-

blende) nature of these epilayers by comparing our results with those on bulk-grown (wurtzite) counterparts. The study also yielded the composition dependence of the zone-center optical-phonon frequencies in these alloys. Photoluminescence at zero magnetic field allowed a determination of the energy gap ( $E_g$ ), whereas the effective  $g$  factor of the band electrons was deduced from its Zeeman shift. In addition, magnetic excitations (Raman EPR and spin flip of donor-bound electrons) were observed in two superlattices containing  $\text{Cd}_{1-x}\text{Mn}_x\text{Se}$  layers.

Recently, we have extended our previous work on  $\text{Cd}_{1-x}\text{Mn}_x\text{Se}$  in several directions. With many MBE-grown samples in the  $0.50 \leq x \leq 0.75$  range and with the introduction of gallium doping, also achieved with MBE, we are now able to study and discuss phenomena over a large concentration spanning  $0 \leq x \leq 0.75$ . We first present results of our reflectivity and photoluminescence studies on the position of the fundamental gap as a function of  $x$ . This extends previous work<sup>7-9</sup> to significantly higher values of  $x$ , allowing a more quantitative assessment of the difference between fundamental gap in the zinc-blende and the wurtzite structures. Furthermore, we have observed additional emission bands close to the  $\text{Mn}^{2+}$  emission in  $\text{Cd}_{1-x}\text{Mn}_x\text{Se}$  epilayers with high  $x$ . We also present and discuss the vibrational Raman spectra of these epilayers, extending our previous results<sup>7</sup> to high values of  $x$ . Finally, the introduction of Ga donors in a controlled manner offers an opportunity to investi-

gate spin-flip Raman signatures of donor-bound electrons in this cubic DMS alloy over a large range of  $x$ , including concentrations where the antiferromagnetic coupling of the  $\text{Mn}^{2+}$  ions cannot be neglected.

## II. EXPERIMENTAL PROCEDURE

### A. Reflectivity

The  $\text{Cd}_{1-x}\text{Mn}_x\text{Se}$  epilayers used in the present study were grown by molecular-beam epitaxy on (001) GaAs substrates. The epilayer thickness ranged from 0.3 to 3.7  $\mu\text{m}$ . The lattice parameter (and therefore the composition) of the samples were determined by x-ray diffraction. The epilayers were found to be of zinc-blende structure, with (001) surfaces (the growth direction is designated by  $z \parallel [001]$  in this paper,  $x$  and  $y$  being taken along  $[100]$  and  $[010]$ , respectively).

In a reflectivity spectrum the onsets of direct and indirect transitions and the associated excitonic features are typically superposed on a strong continuous background. On the other hand, if the sample is subjected to a periodic perturbation (such as piezomodulation) and the reflected light detected with a phase-sensitive lock-in technique, pronounced “derivativelike” signatures are observed in the modulated reflectivity spectrum at energies close to the electronic transitions. The slowly varying background is essentially ignored in the modulated spectrum. The zinc-blende  $\text{Cd}_{1-x}\text{Mn}_x\text{Se}$  epilayers used in our reflectivity study produce a strong interference effect due to multiple reflections from the front surface and the epilayer-substrate interface. Thus strong interference fringes (channeling) occur in the piezomodulated reflectivity spectrum for photon energies less than  $E_g$  where the epilayer is transparent. The occurrence of these fringes obscures the direct observation of excitonic signatures. These interference fringes disappear rather abruptly for photon energies larger than  $E_g$ . It is thus possible to deduce  $E_g$  by merely noting the cessation of the channeled spectrum in a reflectivity spectrum even without resorting to piezomodulation.<sup>8</sup> It is of interest to note that the dispersion of the refractive index can be deduced from the spacings of the interference fringes. From the pronounced increase in the refractive index as the photon energy approaches excitonic transition energies, one can once more deduce  $E_g$ .

In the reflectivity measurements a glass optical cryostat was employed for low-temperature measurements. A Perkin-Elmer (model E-1) double-pass grating monochromator, with a tungsten halogen lamp as a source and an uv-enhanced Si photodiode, constituted the spectrometer. The signal, after digitizing, was acquired with a microcomputer.<sup>10</sup>

### B. Raman scattering

Raman spectra were excited with monochromatic radiation from  $\text{Kr}^+$  or  $\text{Ar}^+$  lasers. The power in the incident beam was typically limited to less than 75 mW in order to avoid sample heating. Measurements in an external magnetic field were carried out using a variable temperature

optical cryostat with a superconducting coil providing external magnetic fields up to 60 kG. Scattered light was spectrally analyzed with a computer-controlled double (triple) SPEX Industries monochromator and detected with standard photon-counting electronics. The photoluminescence measurements were carried out on the same spectrometer.

## III. RESULTS AND DISCUSSION

### A. Reflectivity and photoluminescence

#### 1. Fundamental gap as a function of $x$

As mentioned earlier, the onset of channeling in the reflectivity spectrum observed in the low-energy side of the absorption edge can be used to deduce  $E_g$ .<sup>8</sup> In this manner we have determined  $E_g$  of the zinc-blende  $\text{Cd}_{1-x}\text{Mn}_x\text{Se}$  as a function of  $x$  over a large composition range. We once more emphasize that bulk  $\text{Cd}_{1-x}\text{Mn}_x\text{Se}$  has wurtzite structure, whereas the MBE-grown epilayers exhibit the zinc-blende structure. Figure 1(a) shows the channeling in the reflectivity spectrum of an epilayer of CdSe, while Fig. 1(b) shows it for an epilayer of  $\text{Cd}_{0.25}\text{Mn}_{0.75}\text{Se}$ , both spectra being measured at  $T \approx 10$  K. In Fig. 2 we show the piezomodulated reflectivity spectrum of CdSe, where the free-exciton feature of CdSe at 1.747 eV and the free-exciton signature of GaAs at 1.513 eV are clearly observed. Note that the onset of absorption at 1.75 eV in CdSe [Fig. 1(a)] is in excellent agreement with the value deduced from the position of the signature labeled “CdSe” in the piezomodulated reflectivity spectrum. In Fig. 1(b) the position of the absorption edge at 2.73 eV corresponds to the free-exciton energy of  $\text{Cd}_{0.25}\text{Mn}_{0.75}\text{Se}$ .

Figure 3 shows the index of refraction as a function of energy for zinc-blende CdSe and  $\text{Cd}_{0.25}\text{Mn}_{0.75}\text{Se}$  at  $T = 10$  K. The change in the refractive index with photon energy was calculated from the channeled spectrum, using the layer thickness values of 3.7  $\mu\text{m}$  for CdSe and 3  $\mu\text{m}$  for  $\text{Cd}_{0.25}\text{Mn}_{0.75}\text{Se}$  as estimated from the MBE-growth rates. Near the energy gap there is a steep increase in the index of refraction, as expected from a “single-harmonic oscillator” model. This model assumes that the dispersion of the refractive index is dominated by the free exciton. A least-squares fit with this model yielded  $E_g = 1.75 \pm 0.08$  eV for CdSe and  $E_g = 2.73 \pm 0.08$  eV for  $\text{Cd}_{0.25}\text{Mn}_{0.75}\text{Se}$ , in agreement with the values deduced from the onset of the channeling.

Most DMS's exhibit a linear dependence of the exciton energy with  $x$ , as expected from the virtual-crystal approximation. In some DMS alloys (e.g.,  $\text{Zn}_{1-x}\text{Mn}_x\text{Se}$ ) a downward bowing near low  $x$  has been observed at low temperatures,<sup>11</sup> a behavior attributed to the exchange interaction between the  $\text{Mn}^{2+}$  ion and the band electrons (the so-called “*sp-d* interaction”), which gives rise to corrections in the energy gap in second-order perturbation theory.<sup>12</sup> Figure 4 shows the position of the energy gap in zinc-blende  $\text{Cd}_{1-x}\text{Mn}_x\text{Se}$  as a function of  $x$  at  $T = 10, 80,$  and  $300$  K. A downward bowing in the energy gap versus  $x$  curve can be observed, but in this case

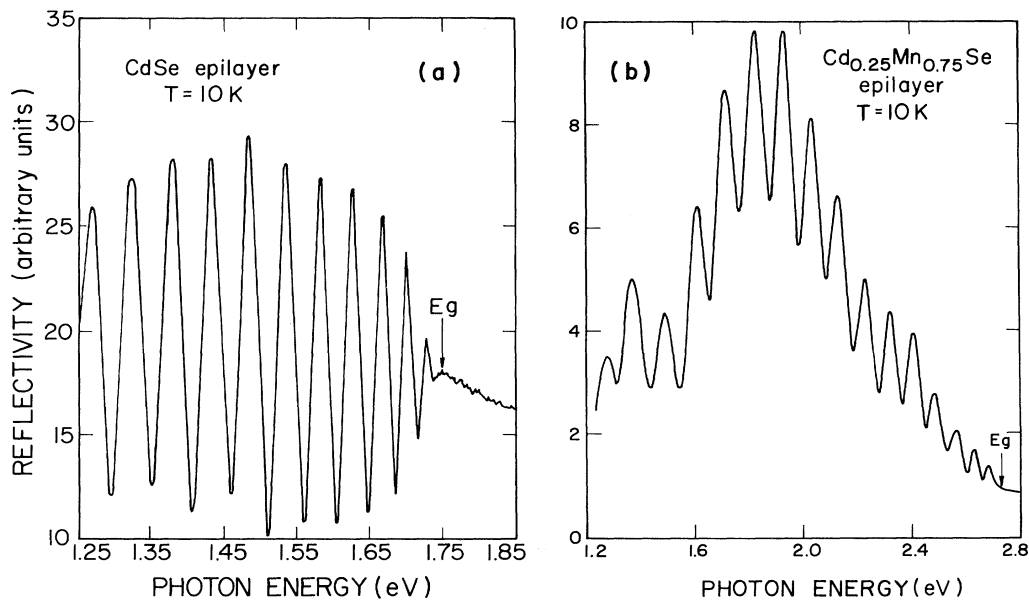


FIG. 1. Reflectivity spectrum of (a) CdSe epilayer and (b)  $\text{Cd}_{1-x}\text{Mn}_x\text{Se}$ ,  $x = 0.75$ . Both spectra were recorded at  $T \sim 10$  K.

the bowing is more pronounced at high  $x$ . On the other hand, for wurtzite  $\text{Cd}_{1-x}\text{Mn}_x\text{Se}$ , this bowing has not been previously observed in the limited range of  $x$  available in bulk [i.e., for  $0 \leq x \leq 0.50$  (Ref. 11)]. It appears that the bowing occurs only in the cubic phase, and may be associated with strain as an additional factor.

Photoluminescence is also a useful technique to obtain

the position of the energy gap in  $\text{Cd}_{1-x}\text{Mn}_x\text{Se}$ , but for  $x > 0.4$  the strong 2.2-eV  $\text{Mn}^{2+}$  luminescence dominates the spectrum, preventing the observation of the excitonic feature. Our previous photoluminescence spectra<sup>7</sup> are in agreement with the reflectivity measurements presented above. Figure 4 shows both the photoluminescence and the reflectivity results on zinc-blende  $\text{Cd}_{1-x}\text{Mn}_x\text{Se}$ . For

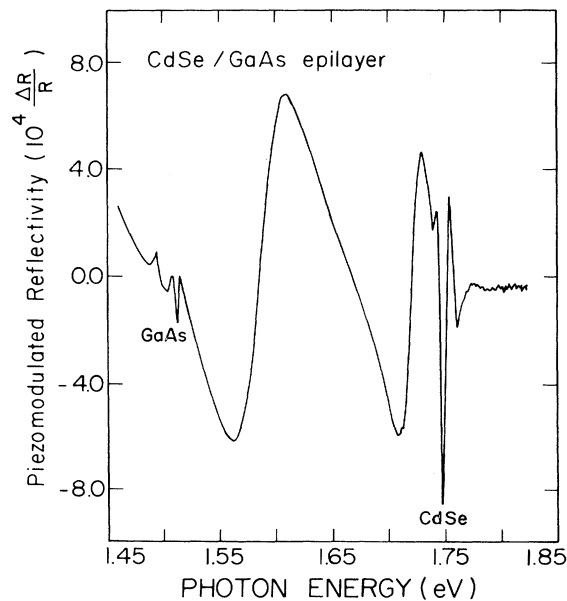


FIG. 2. Piezomodulated reflectivity spectrum of a CdSe epilayer grown on (001) GaAs substrate. The modulated spectrum was recorded at  $T = 10$  K and shows the free-exciton feature of CdSe at 1.747 eV and the free-exciton signature of GaAs at 1.513 eV.

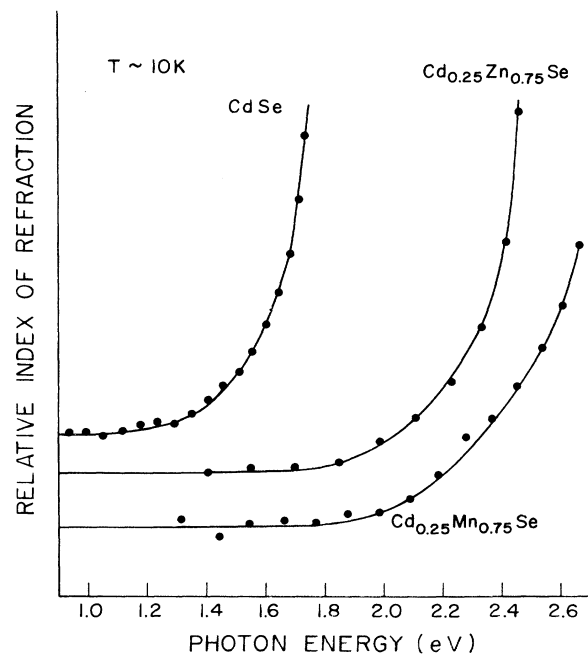


FIG. 3. Index of refraction of CdSe,  $\text{Cd}_{0.25}\text{Zn}_{0.75}\text{Se}$ , and  $\text{Cd}_{0.25}\text{Mn}_{0.75}\text{Se}$  as a function of photon energy.  $T = 10$  K.

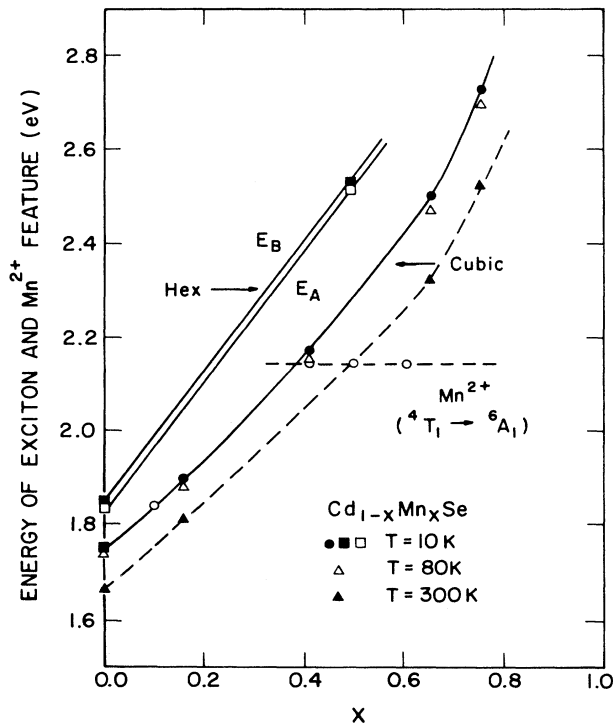


FIG. 4. Energy gap deduced from reflectivity and photoluminescence in zinc-blende  $\text{Cd}_{1-x}\text{Mn}_x\text{Se}$  as function of  $\text{Mn}^{2+}$  concentration  $x$ . The reflectivity measurements were obtained at  $T=10, 80,$  and  $300$  K, while the photoluminescence results are given for  $T=5$  K. For comparison, the energy gap of bulk  $\text{Cd}_{1-x}\text{Mn}_x\text{Se}$  with the wurtzite structure as a function of  $x$  is also included and labeled Hex. The horizontal line denotes the onset of the 2.2-eV  $\text{Mn}^{2+}$  photoluminescence. The points indicated with a square were obtained from piezomodulated reflectivity measurements.

comparison, the reflectivity results on wurtzite  $\text{Cd}_{1-x}\text{Mn}_x\text{Se}$  are also included. We note that the zinc-blende structure differs from the wurtzite in having only one excitonic feature, a smaller energy gap, and a bowing in the  $E_g$  versus  $x$  curve not observed in the hexagonal structure in the range of  $x$  accessible to bulk growth.

## 2. Emission spectra near the $\text{Mn}^{2+}$ ion transition

In the Mn-based DMS's a photoluminescence emission band occurs around 2.2 eV, observed in the Cd-based DMS's only when  $x > 0.4$ . This emission band has been attributed<sup>1</sup> to a transition from the lowest  $^4G$  crystal-field-split excited level to the ground state of  $\text{Mn}^{2+}$  in its tetrahedral environment (see Fig. 5). The  $^4G$  level is split into four levels which are labeled  $^4A_1, ^4E, ^4T_2,$  and  $^4T_1$ , following the group-theoretical notation associated with the symmetry of the crystal field.<sup>1,11</sup> A good review of experimental optical studies of the  $\text{Mn}^{2+}$  levels in II-VI DMS's is given in Ref. 13. The emission spectrum of an epilayer of cubic  $\text{Cd}_{0.4}\text{Mn}_{0.6}\text{Se}$  is shown in Fig. 6. The spectrum was excited at  $T=5$  K with the 4579-Å line of

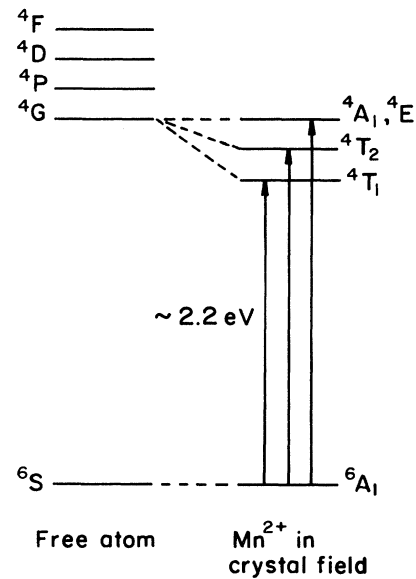


FIG. 5. Intra-ion energy levels of  $\text{Mn}^{2+}$  in the  $T_d$  crystal environment of II-VI DMS's.

an  $\text{Ar}^+$  laser. As can be seen, in addition to the peak labeled *A*, which we associate with the  $^6A_1$ - $^4T_1$  intra-ion transition, two other peaks *B* and *C* are observed on the high-energy side of *A*.

Peaks *B* and *C*, also observed in  $\text{Cd}_{0.5}\text{Mn}_{0.5}\text{Se}$ , are tentatively interpreted as impurity levels. Although these impurities have yet to be identified, we describe some of their characteristics, since their eventual identification is important in the context of MBE growth of II-VI compounds, where the control of defects is clearly desirable.

Figure 7 shows the temperature dependence of the energies of *A*, *B*, and *C* showing, at low temperatures, a

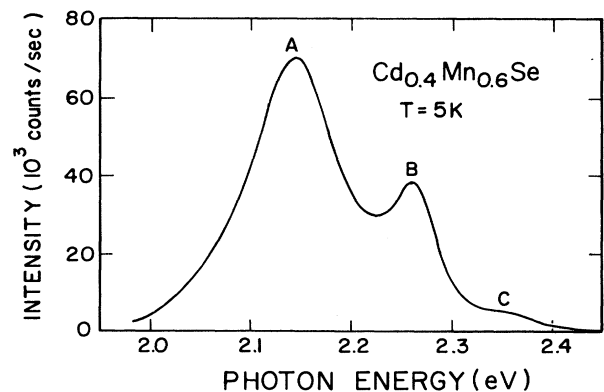


FIG. 6. Photoluminescence emission spectrum of  $\text{Cd}_{1-x}\text{Mn}_x\text{Se}$ ,  $x=0.60$ , at  $T=5$  K. The spectrum was excited with the laser line  $\lambda_L=4579$  Å having a power of 3.6 mW. The peak *A* corresponds to the  $^6A_1$ - $^4T_1$  intra-ion transition of  $\text{Mn}^{2+}$ , while the peaks *B* and *C* are attributed to emission from impurity levels.

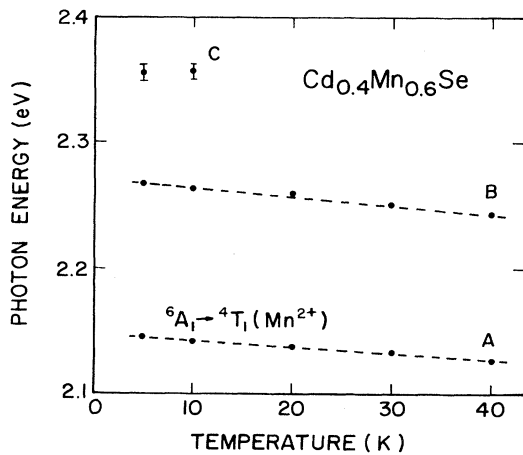


FIG. 7. Temperature dependence of the emission peak energies in  $\text{Cd}_{0.4}\text{Mn}_{0.6}\text{Se}$ . The emission spectra were excited with  $\lambda_L = 5145 \text{ \AA}$ .

negative slope with increasing temperature. Although the  ${}^6A_1-{}^4T_2$  and  ${}^6A_1-{}^4A_1, {}^4E$  transitions are expected to have a similar temperature dependence and energies as those of *B* and *C* (Refs. 14 and 15; see also Table I for comparison with other DMS's), their assignments based on this behavior have to be discounted for the following reasons: First, it is unlikely that the higher levels will be populated sufficiently to produce observable emission. Second, the result of a "pseudoexcitation" experiment, described below, does not support such an interpretation.

The energies of the  $\text{Mn}^{2+}$  transitions obtained from emission are lower than those obtained from absorption because the emission is shifted to longer wavelength due to lattice relaxation.<sup>16</sup> This Stokes-shifted emission is un-

derstood in simple terms from a configuration coordinate diagram associated with a localized emission center. If the emission is from a band, a momentum diagram is more appropriate and, in principle, there is no difference between the absorption and emission energies, except for the possible involvement of crystal excitations such as phonons.

Based on previous measurements on absorption and emission peaks in several DMS systems,<sup>13</sup> we can estimate the position of the absorption features of the  ${}^4G$  split levels of  $\text{Mn}^{2+}$  in  $\text{Cd}_{0.4}\text{Mn}_{0.6}\text{Se}$ . A pseudoexcitation experiment was carried out by exciting the luminescence of a given peak with energies both above and below the corresponding absorption; if the peak is to be associated with a localized level of  $\text{Mn}^{2+}$ , it should be observed only when the exciting energy is above the corresponding absorption peak. This was found to be the case for line *A*, but not for *B* and *C*, indicating that only *A* can be associated with the  $\text{Mn}^{2+}$  absorption. We thus tentatively assign peaks *B* and *C* to unknown deep impurity levels in the band gap, with emission energies exceeding that of the  $\text{Mn}^{2+}$  lowest transition. These impurities are most likely different from the donors giving rise to the spin-flip Raman scattering from donor-bound electrons (see Sec. III C 2 below), since peaks *B* and *C* do not exhibit the large Zeeman shift characteristic of the exciton and shallow levels.

Peak *B* has an interesting behavior as a function of incident intensity. For low intensities (less than 3 mW), it is very weak. As the incident intensity is increased, the intensity of *A* increases linearly, but that of *B* increases much faster, overtaking the intensity of *A* at about 5.5 mW, as displayed in Fig. 8. A nonlinear behavior often appears in association with competing channels of decay, energy-transfer mechanisms, or saturation processes.

TABLE I. Interband  $3d$  transitions of  $\text{Mn}^{2+}$  in a  $T_d$  crystal field. The transition energies are given in eV. The values marked with an asterisk correspond to the emission peaks attributed to deep impurities. The values for  $\text{Zn}_{0.65}\text{Mn}_{0.35}\text{Se}$  are given for parallel polarization; the values for perpendicular polarization are somewhat higher. For a more complete table including other DMS's see Ref. 13. All information is given for  $T = 5 \text{ K}$ .

Alloy	$x$	${}^6A_1-{}^4T_1$	${}^6A_1-{}^4T_2$	${}^6A_1-{}^4A_1, {}^4E$	Reference
$\text{Cd}_{1-x}\text{Mn}_x\text{Se}$					
Emission	0.50	2.141	2.256*		Present work
	0.60	2.144	2.260*	2.350*	Present work
	0.45	2.13			Moriwaki <i>et al.</i> (Ref. 27)
Absorption	0.45	2.3			Morales <i>et al.</i> (Ref. 28)
	0.48	2.3			Morales <i>et al.</i> (Ref. 28)
$\text{Zn}_{1-x}\text{Mn}_x\text{Se}$					
Absorption	0.23	2.380	2.510	2.680	Morales <i>et al.</i> (Ref. 29)
	0.35	2.393	2.522	2.864	Morales <i>et al.</i> (Ref. 29)

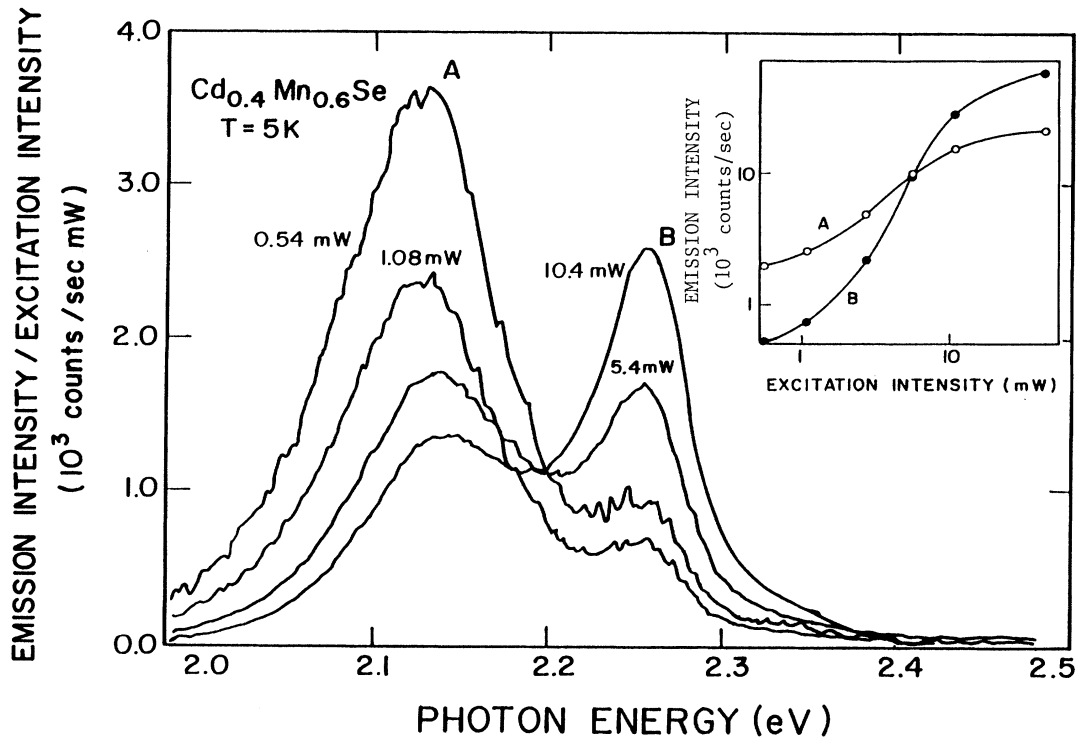


FIG. 8. Relative intensity of the  $\text{Mn}^{2+}$  emission spectra as a function of the incident intensity.

The mechanism in this particular case has yet to be established, and further experimental studies are needed in order to determine the origin of *B* and *C*. In this context, (i) excitation photoluminescence, where the emission peaks can be associated with the corresponding absorption peaks; (ii) direct absorption measurements, which have been exploited<sup>13</sup> for locating the  $^4G$  split levels of  $\text{Mn}^{2+}$  in the other DMS alloys (its application to the epilayers would require removing the GaAs substrate by etching); and (iii) time-resolved photoluminescence, useful in identifying the competing centers, appear particularly promising.

### 3. Effect of a magnetic field on the energy gap

As mentioned earlier, excitonic photoluminescence can be observed, unobscured by the intra- $\text{Mn}^{2+}$  transitions, for  $x < 0.4$ .<sup>7</sup> From a study of its Zeeman effect one can deduce the effective *g* factors characterizing the band extrema. It is of interest to carry out this study in a doped crystal, since in addition to excitonic luminescence, spin flip of donor-bound electrons can then also be observed. This in turn permits a comparison of the Zeeman shifts of the exciton and of the conduction band (see Sec. III C 2). For this study we choose a Ga-doped epilayer of cubic  $\text{Cd}_{0.9}\text{Mn}_{0.1}\text{Se}$ , since hexagonal  $\text{Cd}_{0.9}\text{Mn}_{0.1}\text{Se}$  has been previously studied,<sup>17-19</sup> thus allowing a direct comparison of the phenomenon in the zinc-blende and wurtzite structures.

The photoluminescence spectrum of a  $\text{Cd}_{0.9}\text{Mn}_{0.1}\text{Se}:\text{Ga}$  epilayer, at  $T = 5$  K with incident wave-

length of  $4880 \text{ \AA}$ , is shown in Fig. 9 for  $H = 0$  and 60 kG. The position of the exciton peak at 1.861 eV for  $H = 0$  is consistent with the results shown in Fig. 4.

The magnetic field shift of the photoluminescence peak is large, as is typical for DMS's. The Zeeman shift of the *A* exciton is given by the expression  $\Delta E = \frac{1}{2}N_0(\alpha - \beta)\bar{x}\langle S \rangle$ , where  $\alpha$  and  $\beta$  are the conduction- and valence-band exchange integrals,  $\bar{x}$  is the concentration of  $\text{Mn}^{2+}$  ions that contribute to the magnetization, and  $\langle S \rangle$  is the magnitude of the thermal average of  $\text{Mn}^{2+}$  spins.<sup>19</sup> In the linear (low-field) region

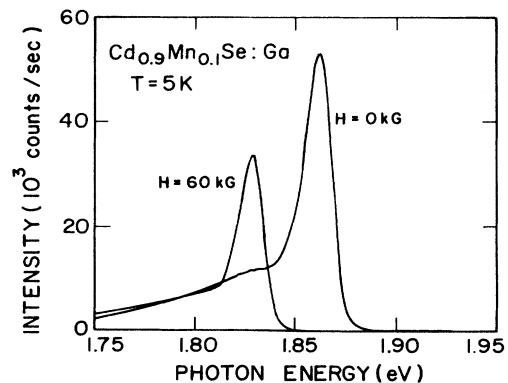


FIG. 9. Photoluminescence spectrum of an epilayer of cubic (zinc-blende)  $\text{Cd}_{1-x}\text{Mn}_x\text{Se}$ ,  $x = 0.10$ , at  $T = 5$  K, with  $\lambda_L = 4880 \text{ \AA}$ , for  $H = 0$  and 60 kG.

TABLE II. The  $g$  factors associated with the energy gap ( $E_{\text{gap}}$ ) and the conduction band in  $\text{Cd}_{1-x}\text{Mn}_x\text{Se}$  at  $T=5$  K.

Symmetry	$x$	$g_{\text{eff}}(E_{\text{gap}})$	$g_{\text{eff}}(\text{Conduction band})$	Impurity	
Zinc blende	0.10	106.1	93.7	Ga	
	0.16	159.7			
	0.41	52.5			
	0.50			30.1	unknown
	0.60			30.0	unknown
	0.65			23.1	unknown
	0.75			20.1	unknown
Wurtzite	0.10	180 <sup>a</sup>	94.3 <sup>b</sup>	In	
	0.10	280 <sup>c</sup>			
	0.30		67.2 <sup>b</sup>	In	

<sup>a</sup>Photoluminescence data for  $\mathbf{H}\parallel c$  (Ref. 17).

<sup>b</sup>Spin-flip data (Ref. 18).

<sup>c</sup>Value at 5 K calculated from magnetorefectance data at 1.5 K given in Ref. 19. The difference between the magnetorefectance and photoluminescence results for  $x=0.1$  is not clear.

$\Delta E = g\mu_B H$ . Based on this we obtain a  $g$  factor of 106 at 5 K (see the third column of Table II).

It is of interest to compare the magnitude of the Zeeman splittings in the wurtzite and zinc-blende structures for the same  $x$  (see Table II). The  $g$  factor for wurtzite  $\text{Cd}_{0.9}\text{Mn}_{0.1}\text{Se}$  at  $T=5$  K, previously obtained from the photoluminescence of the donor-bound exciton, is  $g_{\text{hex}} \sim 180$  (for  $\mathbf{H}\parallel c$ ),<sup>17</sup> somewhat larger than that for the cubic structure. These differences can be attributed to different values of  $(\alpha - \beta)$  in the two structures.<sup>20</sup>

### B. Vibrational Raman spectra

In this section we present a Raman-scattering study of the vibrational modes of cubic  $\text{Cd}_{1-x}\text{Mn}_x\text{Se}$  epilayers, which extends our previous work<sup>7</sup> where the maximum  $x$  investigated was 0.41. The increase in  $x$  up to 0.75, now available, allowed us to extend the study (and thus the

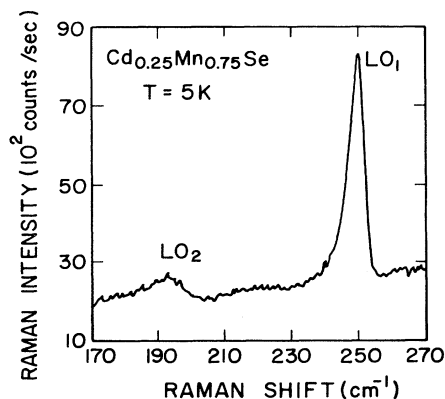


FIG. 10. Raman spectrum of a (001) epilayer of zinc-blende  $\text{Cd}_{1-x}\text{Mn}_x\text{Se}$ ,  $x=0.75$ , at  $T=5$  K. The spectrum was recorded in the backscattering geometry  $z(xx)\bar{z}$  with  $\lambda_L=4965$  Å. The peaks observed are associated with the zone center  $\text{LO}_1$  and  $\text{LO}_2$  optical phonons.

understanding of the cubic  $\text{Cd}_{1-x}\text{Mn}_x\text{Se}$  alloy system) significantly.

Figure 10 shows the Raman spectrum of a (001) epilayer of cubic  $\text{Cd}_{1-x}\text{Mn}_x\text{Se}$ ,  $x=0.75$ , recorded in the backscattering geometry  $z(xx)\bar{z}$ . The spectrum was recorded at 5 K using the 4579-Å line of the  $\text{Ar}^+$  laser. The Raman peak labeled  $\text{LO}_2$  can be traced to the zone-center LO phonon of CdSe as  $x \rightarrow 0$ , whereas that labeled  $\text{LO}_1$  evolves from the local mode of  $\text{Mn}^{2+}$  in CdSe as  $x$  increases (and extrapolates to the LO-phonon mode of cubic MnSe as  $x \rightarrow 1$ ). These extrapolations can be appreciated from the frequencies of the relevant Raman lines as a function of  $x$  displayed in Fig. 11.

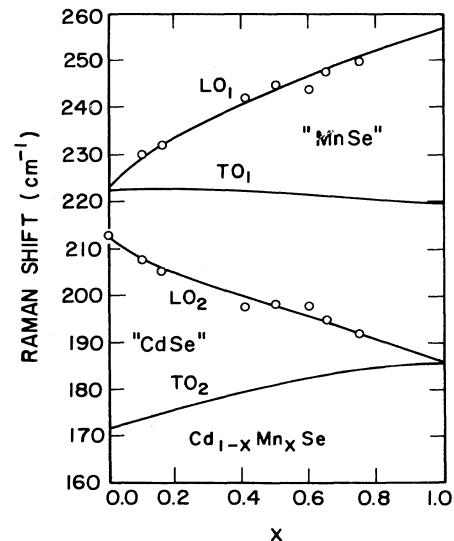


FIG. 11. Composition dependence of the zone-center optical-phonon frequencies in zinc-blende  $\text{Cd}_{1-x}\text{Mn}_x\text{Se}$ . The solid lines were calculated with the MREI model for mixed crystals (Ref. 21). The assignments of the modes follow the scheme in Genzel *et al.* (Ref. 22).

In Fig. 11 the optical phonons of  $\text{Cd}_{1-x}\text{Mn}_x\text{Se}$  show a composition dependence corresponding to a “two-mode” behavior. In the two-mode behavior the modes (LO and TO) of each of the two binary crystals involved in the alloy maintain their character throughout the concentration range and are referred to as “CdSe” modes and “MnSe” modes. As  $x \rightarrow 1$ , the CdSe-mode frequencies extrapolate to that of the gap mode of Cd in MnSe. On the other hand, as already mentioned above, the MnSe modes at  $x = 1$  become the local mode of  $\text{Mn}^{2+}$  in CdSe as  $x \rightarrow 0$ . At  $x = 0$ , the local mode of  $\text{Mn}^{2+}$  in CdSe has a frequency higher than those of the two modes of CdSe, as expected from the fact that the  $\text{Mn}^{2+}$  mass is significantly smaller than that of Cd.

The calculated curves in Fig. 11 are generated from a modified-random-element-isodisplacement (MREI) model.<sup>7,21,22</sup> The macroscopic parameters used in the model are listed in our previous paper (see Table III in Ref. 7). The data points for high  $x$  obtained in the present study modified our previous estimate of the frequency of the impurity mode of Cd in the hypothetical MnSe crystal, i.e., of  $\omega_I(\text{MnSe}:\text{Cd})$ , from 180 to 186  $\text{cm}^{-1}$ . This necessitated only a small correction in the force constants obtained from the MREI model.<sup>23</sup> The additional data give a more quantitative picture of the compositional dependence of the two-mode behavior.

We refer the reader to our previous work<sup>7</sup> for additional comments on the vibrational spectra of cubic  $\text{Cd}_{1-x}\text{Mn}_x\text{Se}$ , such as the MREI model as applied to the present case, a comparison with the “intermediate-mode” behavior observed in  $\text{Zn}_{1-x}\text{Mn}_x\text{Se}$ , and a comparison between the frequencies of the zone-center Raman lines observed in cubic and uniaxial<sup>17</sup>  $\text{Cd}_{1-x}\text{Mn}_x\text{Se}$ .

### C. Raman studies of *sp-d* exchange

In the absence of direct magnetic measurements (which are not available at this time, and are quantitatively difficult due to the unavoidable contribution of the substrate), optical spin-flip studies provide us with the only information on the magnetization  $M(H, T, x)$  in these layered systems. In this section we present a Raman-scattering study of the *sp-d* exchange interaction in the zinc-blende epilayers of  $\text{Cd}_{1-x}\text{Mn}_x\text{Se}$  as manifested in the spin-flip of donor-bound electrons. In the first part we estimate the value for the ratio of the *sp-d* exchange constants  $\alpha/\beta$  based on the spin-flip Raman and photoluminescence measurements. In the second part we focus on the behavior of the spin-flip Raman shift in crystals with  $x > 0.4$ , where significant antiferromagnetic ordering can occur.

#### 1. Spin-flip from electrons bound to donors

A striking Raman feature associated with magnetic excitations encountered in a DMS is the spin flip of electrons bound to donors, enhanced by the *s-d* exchange interaction. Figure 12 shows the Raman spectrum of zinc-blende  $\text{Cd}_{1-x}\text{Mn}_x\text{Se}$ ,  $x = 0.10$ , doped with Ga, where such a spin-flip Raman line is observed. The spectrum is obtained at 5 K in the backscattering configuration

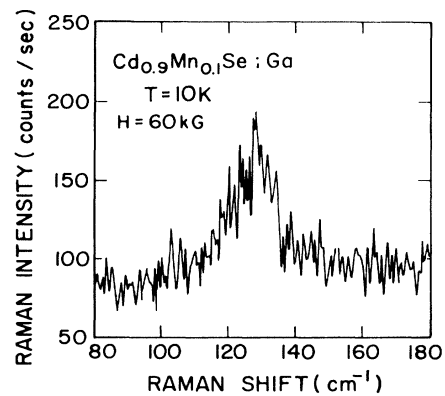


FIG. 12. Raman spectrum associated with the spin-flip of electrons bound to donors in  $\text{Cd}_{0.9}\text{Mn}_{0.1}\text{Se}:\text{Ga}$  epilayer. The spectrum is obtained at  $T = 5$  K in the crossed polarization  $z(yx)\bar{z}$ , with  $H = 60$  kG along  $x$  and  $\lambda_L = 6471$  Å.

$z(xy)\bar{z}$ , with a magnetic field of 60 kG along  $x$ . As in a bulk DMS, the Raman shift of the donor spin-flip line exhibits a Brillouin-function-like behavior, as can be seen in Fig. 13. Since the spin-flip Raman mechanism also involves interband electronic transitions,<sup>6</sup> one observes a resonant enhancement for incident frequencies close to excitonic excitations.

The spin splitting of the donor ground state in DMS's

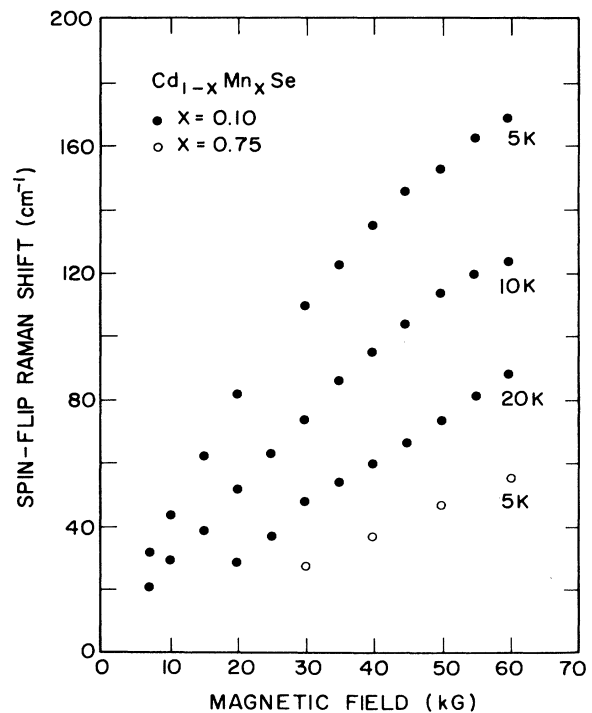


FIG. 13. Magnetic field and temperature dependence of the spin-flip Raman shift in the  $\text{Cd}_{0.9}\text{Mn}_{0.1}\text{Se}:\text{Ga}$  and  $\text{Cd}_{0.25}\text{Mn}_{0.75}\text{Se}$  epilayers, with external magnetic field in the plane of the (001) layers. The spectra were obtained in the cross polarization  $z(xy)\bar{z}$  with  $\lambda_L = 6471$  Å.

is determined by the macroscopic magnetization of the  $\text{Mn}^{2+}$  ions and the “intrinsic” Zeeman effect, i.e.,

$$\hbar\omega_{\text{SFR}} = \frac{\alpha}{\mu_B g_{\text{Mn}^{2+}}} M_0(H) + g^* \mu_B H = g_{\text{eff}} \mu_B H, \quad (1)$$

where  $\alpha$  is the exchange integral characterizing the interaction between the spins of  $\text{Mn}^{2+}$  ions and those of the  $s$ -like  $\Gamma_6$  electrons;  $\mu_B$  is the Bohr magneton;  $M_0(H)$  is the macroscopic magnetization;  $g_{\text{Mn}^{2+}} = 2$  is the  $g$  factor of  $\text{Mn}^{2+}$ ;  $g^*$  is the intrinsic  $g$  factor of the band electrons; and  $g_{\text{eff}}$  is the effective  $g$  factor of the conduction band, consisting of the sum of the two preceding mechanisms. Because of the strong  $s$ - $d$  exchange interaction, the term involving  $\alpha$  in Eq. (1) dominates the spin splitting.<sup>18</sup> The spin splitting can also be written in a form which makes explicit the behavior as a function of temperature and magnetic field, i.e.,

$$\hbar\omega_{\text{SFR}} = \frac{5}{2} \bar{\alpha} N_0 B_{5/2}(g \mu_B H / k_B T) + g^* \mu_B H, \quad (2)$$

where  $B_{5/2}$  is the Brillouin function  $B_J$  for  $J = \frac{5}{2}$ , and  $N_0$  is the density of cations.

From the slope of the linear (low-field) portion of the spin-flip data for zinc-blende  $\text{Cd}_{0.9}\text{Mn}_{0.1}\text{Se}:\text{Ga}$  shown in Fig. 13, we obtain  $g_{\text{eff}} = 94$  at 5 K, which is consistent with that observed in bulk (wurtzite)  $\text{Cd}_{0.9}\text{Mn}_{0.1}\text{Se}$  within experimental error (see Table II). This seems to indicate that the exchange constant  $\alpha$  has a comparable value in both the wurtzite and the zinc-blende structures. This is to be expected, since the number of nearest neighbors and the cation-cation distance—both of which determine magnetization—are the same in both structures.

The results on the magnetic-field dependence of the low-energy excitonic peak observed in photoluminescence, discussed in Sec. III A 3 (see also Table II), indicated that  $(\alpha - \beta)$  in wurtzite  $\text{Cd}_{0.9}\text{Mn}_{0.1}\text{Se}$  is larger than that in the zinc-blende epilayer. Since the values of  $\alpha$  are the same, this difference has to be attributed to a difference in the values of  $\beta$ . From the spin-flip and photoluminescence measurement we obtain  $|\alpha/\beta|_{\text{hex}} = 0.57$  and  $|\alpha/\beta|_{\text{cub}} = 0.80$ . The values for  $|\alpha/\beta|_{\text{hex}}$  previously reported are 0.22,<sup>24</sup> 0.23,<sup>19</sup> and 0.4.<sup>25</sup> As pointed out in an earlier section, this discrepancy needs to be resolved.

## 2. Spin-flip Raman shift in high- $x$ crystals

An important aspect of spin-flip Raman scattering is its dependence on the Mn concentration. Here we focus on zinc-blende  $\text{Cd}_{1-x}\text{Mn}_x\text{Se}$  with high  $\text{Mn}^{2+}$  concentration, with  $x$  in the range  $0.50 \leq x \leq 0.75$ —a region which, before the MBE growth, was not accessible for this alloy—where the antiferromagnetic interactions between neighboring  $\text{Mn}^{2+}$  ions become important. This is well above the concentration required for the onset of lattice frustration ( $x_{\text{percolation}} = 0.17$ – $0.19$ ) and the occurrence of the spin-glass phase.

Figure 14 shows the Raman spectrum of zinc-blende  $\text{Cd}_{1-x}\text{Mn}_x\text{Se}$ ,  $x = 0.60$ , where a Raman line consistent with spin-flip is observed. The spectrum is obtained at 5 K in the backscattering configuration  $z(xy)\bar{z}$ , with a magnetic field of 60 kG along  $x$ . This Raman line shows a

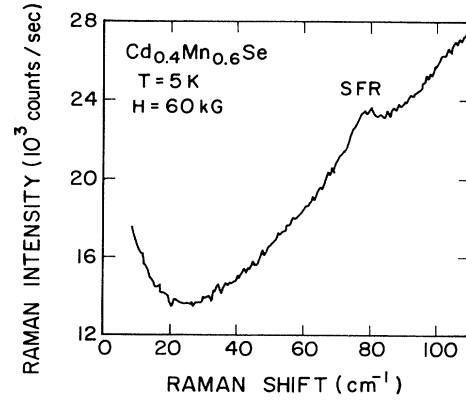


FIG. 14. Raman spectrum associated with the spin-flip of electrons bound to donors in  $\text{Cd}_{0.4}\text{Mn}_{0.6}\text{Se}$  epilayer. The spectrum is obtained at  $T = 5$  K in the crossed polarization  $z(\gamma x)\bar{z}$ , with  $H = 60$  kG along  $x$  and  $\lambda_L = 6471$  Å.

linear dependence on magnetic field, as can be seen from the data included in Fig. 13, and a weak dependence on temperature. This sample was not intentionally doped, but exhibits  $n$ -type properties due to the presence of unknown donors. The spin-flip Raman shifts for  $x = 0.60$  correspond to a  $g$  factor of 30. The  $x$  dependence of the conduction-band  $g$  factor is given in Table II.

The  $x$  dependence of spin-flip Raman scattering reflects the dependence of the magnetization on the composition  $x$ , in addition to its Brillouin-function-like behavior with  $H$  and  $T$ . The manner in which the magnetization enters the  $g$  factor is shown explicitly in Eq. (1).

Figure 15 shows the  $x$  dependence of the  $g$  factor ob-

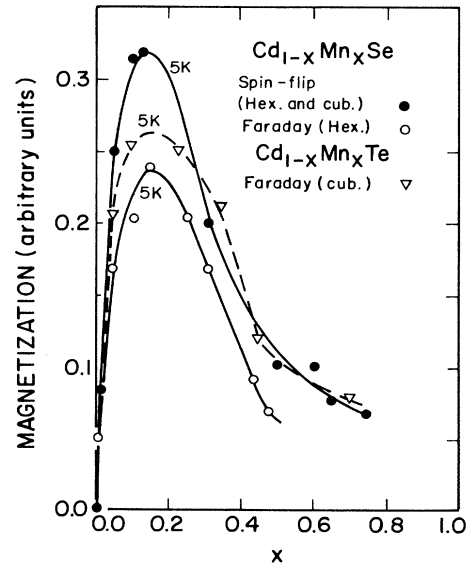


FIG. 15. Comparison between the  $x$  dependence of the magnetization deduced from spin-flip Raman shift of donor-bound electrons (solid circles) and that deduced from Faraday-rotation experiments (open triangles and circles); the  $x$  dependence of the magnetization is deduced from the  $x$  dependence of the Verdet constant as reported by Oh *et al.* in Ref. 2(c).

tained from spin-flip Raman scattering. The shape of the curve is due to the  $x$  dependence of the magnetization which, for small  $x$ , increases with increasing  $x$ , but for higher  $x$  shows a striking decrease due to the antiferromagnetic interaction between the larger concentration of  $\text{Mn}^{2+}$  neighbors. It is interesting to compare this behavior with Faraday rotation, which also depends on the magnetization  $M(H, T, x)$  in a similar manner,<sup>2</sup> and we include in the figure the Faraday-rotation data observed at the same temperature in bulk hexagonal  $\text{Cd}_{1-x}\text{Mn}_x\text{Se}$  and bulk cubic  $\text{Cd}_{1-x}\text{Mn}_x\text{Te}$  over a similar range of  $x$ .

It is clear that Eq. (2) for the spin-flip Raman shift in low- $x$  crystals cannot describe the weak temperature dependence of the spin-flip Raman shift observed in high- $x$  samples. It has been previously proposed<sup>18</sup> that Eq. (2) should be modified by replacing  $T$  by  $T + T_{\text{AF}}$ , where  $T_{\text{AF}}$  is a phenomenological constant inserted to account for weak antiferromagnetic interactions. This approach allows an interpretation of the data very well up to  $x = 0.75$ , where the antiferromagnetic effects are expected to be very strong. An estimate of the antiferromagnetic temperature  $T_{\text{AF}}$  and the effective  $\text{Mn}^{2+}$  concentration  $\bar{x}$  can be obtained by using the mean-field approximation; these parameters describe the deviation from the paramagnetic behavior,  $T_{\text{AF}} > 0$  and  $\bar{x} < x$ , in a more quantitative manner.

In the mean-field approximation, we neglect the bound-magnetic-polaron energy, and consider only those portions of the Raman-shift data that are linear in the magnetic field. In this approximation,

$$\hbar\omega_{\text{SFR}} = \Delta_x = \frac{\alpha}{g\mu_B} M_0(H, T, x) \sim \frac{35\bar{x}(\alpha N_0)}{12k_B(T + T_{\text{AF}})} g\mu_B H. \quad (3)$$

Hence the effective  $g$  is

$$g_{\text{eff}} = \frac{1}{\mu_B} \frac{d\Delta_x}{dH} \sim \frac{35\bar{x}(\alpha N_0)}{12k_B(T + T_{\text{AF}})} g + g^* = g_x + g^*.$$

In order to determine  $\bar{x}(\alpha N_0)$  and  $T_{\text{AF}}$  for each sample, the values of  $(1/g_{\text{eff}})$  as determined from the slope of the  $\Delta_x$  versus  $H$  curves are plotted in Fig. 16. All the samples show a linear dependence given by

$$\frac{1}{g_{\text{eff}}} = m(T + T_{\text{AF}}) \text{ for } T \leq 40 \text{ K}.$$

From these plots, a least-squares fit was used to determine  $T_{\text{AF}}$  and  $m$ , the latter being proportional to  $(\bar{x}\alpha N_0)^{-1}$ . These results are summarized in the lower part of Table III. For comparison, in Table III we also give the values for  $N_0$  and  $T_{\text{AF}}$  in the hexagonal  $\text{Cd}_{1-x}\text{Mn}_x\text{Se}$ .<sup>18</sup> For a given  $x$  the values of these parameters do not differ much, as would be expected, since the magnetic sublattices are the same in both structures in terms of nearest-neighbor interactions.

The parameters  $\bar{x}\alpha N_0$  and  $T_{\text{AF}}$  listed in Table III exhibit some general trends. As expected,  $\bar{x}\alpha N_0$  and  $T_{\text{AF}}$  increase with  $x$ . The antiferromagnetic temperature  $T_{\text{AF}}$  shows a gradual increase with  $x$  up to  $x \sim 0.25$ ;<sup>18</sup> when  $x$  exceeds this value, there is clearly a dramatic increase in

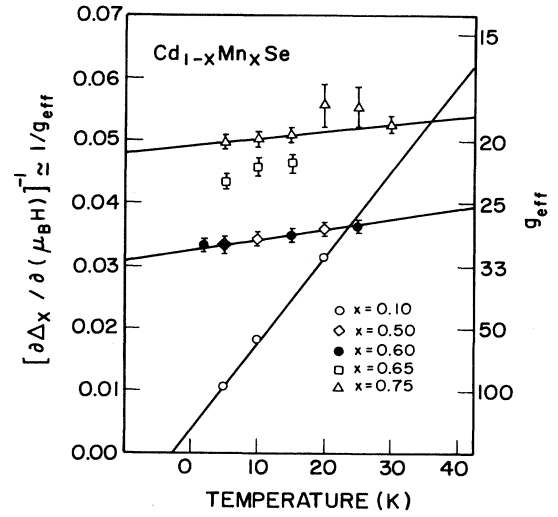


FIG. 16.  $\mu_B(d\Delta_x/dH)^{-1}$  vs temperature in the  $\text{Cd}_{1-x}\text{Mn}_x\text{Se}$  epilayers.  $d\Delta_x/dH$  is the slope of the linear portion of the Raman shift vs  $H$ , where the intrinsic Zeeman contribution has been subtracted. The straight lines are fits to the experimental data. See Table III for parameters.

$T_{\text{AF}}$  showing a clear difference between low- $x$  samples below percolation and high- $x$  samples above percolation for which there is presently no theory to describe  $M(H, T, x)$  below the critical temperature  $T_g$ .<sup>1</sup> The increase of  $T_{\text{AF}}$  with increasing  $x$  can be correlated to the corresponding increase of the strength of the antiferromagnetic coupling. We note that the hexagonal bulk phase has not been grown for  $x > 0.50$ , so that higher  $x$  values are available only in the zinc-blende phase of  $\text{Cd}_{1-x}\text{Mn}_x\text{Se}$ . Note that  $T_{\text{AF}}$  for  $x = 0.75$  is, remarkably,  $\sim 450$  K. Since  $T_{\text{AF}}$  was introduced as a phenomenological term for the low- $x$  limit [see Eq. (3)], it is interesting that  $(g_{\text{eff}})^{-1}$  is linear with  $T$  even for very high concentrations. Qualitatively similar behavior was also noted in Ref. 26, where  $T_{\text{AF}}$  deduced from Faraday rotation of high-Mn-concentration  $\text{Cd}_{1-x}\text{Mn}_x\text{Te}$  indicated a very large  $T_{\text{AF}}$  for  $x \sim 0.70$ .

TABLE III. Parameters for spin-flip curve fitting in  $\text{Cd}_{1-x}\text{Mn}_x\text{Se}$ .

Symmetry	$x$	$\bar{x}\alpha N_0$ (meV)	$T_{\text{AF}}$ (K)
Wurtzite <sup>a</sup>	0.01	2.18	0.85
	0.05	7.06	1.38
	0.10	10.1	2.28
	0.13	11.5	3.10
	0.31	16.2	13.3
Zinc blende	0.10	10.7	2.8
	0.50	89.0	195.1
	0.60	90.5	199.3
	0.65		
	0.75	134.1	446.8

<sup>a</sup>Reference 18.

#### IV. CONCLUDING REMARKS

The Raman scattering, emission, and reflectivity studies reported in this paper for the zinc-blende  $\text{Cd}_{1-x}\text{Mn}_x\text{Se}$  epilayers extend the previous investigation on this DMS now available by MBE growth up to  $x \leq 0.75$ . Here we present a study which includes the  $x$  dependence of the energy gap, impurity emission near the 2.2-eV transition of  $\text{Mn}^{2+}$ , Zeeman shifts of the conduction and valence bands, and associated exchange constants, and we give special attention to the investigation of spin-flip of donor-bound electrons in the high-manganese-concentration range. The energy gap  $E_g(x)$  in the zinc-blende structure is smaller than that for the wurtzite structure throughout the investigated range of compositions, and shows a downward bowing, a feature which could be attributed to the strains arising when a crystal which naturally grows with wurtzite symmetry is forced to assume a zinc-blende structure. The spin-flip studies indicate large values of  $T_{\text{AF}}$  for high- $x$  crystals, a clear evidence of antiferromagnetic ordering, typical of DMS. This adds to the list of DMS's where magnetic order can be addressed experimentally. Attempts to observe a magnon signature  $\omega_M$  have not yet been success-

ful, detectable peak intensities requiring larger scattering volumes than typically available in an epilayer. Perhaps the use of multichannel detection such as is feasible with charge-coupled devices, which allow large integration times, may make such studies more accessible. The present study sets the stage for the investigation of heterostructures based on this alloy. Superlattices and single quantum wells involving  $\text{Cd}_{1-x}\text{Mn}_x\text{Se}$  have already been grown and our preliminary results indicate that their structural quality is quite good.

#### ACKNOWLEDGMENTS

We greatly appreciate useful comments on the Mn levels made to us by W. M. Becker and J. F. MacKay. The work reported in this paper was carried out with support from the Defense Advanced Research Projects Agency-University Research Initiative Consortium on Submicron Heterostructures and Optical Electronics in Wide-Gap II-VI Semiconductors and Related Compounds, administered by the Office of Naval Research (N00014-86-K-0760). The work at Purdue and University of Notre Dame also received support from the National Science Foundation, Grants Nos. DMR-89-21717 and DMR-89-13706, respectively.

\*Present address: Kodak Research Laboratory, Eastman Kodak Company, Rochester, NY 14650.

<sup>1</sup>J. K. Furdyna, *J. Appl. Phys.* **64**, R29 (1988).

<sup>2</sup>(a) J. A. Gaj, R. R. Galazka, and M. Nawrocki, *Solid State Commun.* **25**, 193 (1978); (b) D. U. Bartholomew, J. K. Furdyna, and A. K. Ramdas, *Phys. Rev. B* **34**, 6943 (1986); (c) Eunsoo Oh, D. U. Bartholomew, A. K. Ramdas, J. K. Furdyna, and U. Debska, *ibid.* **38**, 13 183 (1988).

<sup>3</sup>See the article by A. K. Ramdas and S. Rodriguez, in *Diluted Magnetic Semiconductors*, Vol. 25 of *Semiconductors and Semimetals*, edited by R. K. Willardson and A. C. Beer (Academic, New York, 1988), p. 345.

<sup>4</sup>D. U. Bartholomew, E.-K. Suh, S. Rodriguez, A. K. Ramdas, and R. L. Aggarwal, *Solid State Commun.* **62**, 235 (1987).

<sup>5</sup>S. Venugopalan, A. Petrou, R. R. Galazka, A. K. Ramdas, and S. Rodriguez, *Phys. Rev. B* **25**, 2681 (1982).

<sup>6</sup>A. Petrou, D. L. Peterson, S. Venugopalan, R. R. Galazka, A. K. Ramdas, and S. Rodriguez, *Phys. Rev. B* **27**, 3471 (1983).

<sup>7</sup>R. G. Alonso, E.-K. Suh, A. K. Ramdas, N. Samarth, H. Luo, and J. K. Furdyna, *Phys. Rev. B* **40**, 3720 (1989).

<sup>8</sup>N. Samarth, H. Luo, J. K. Furdyna, S. B. Qadri, Y. R. Lee, A. K. Ramdas, and N. Otsuka, *Appl. Phys. Lett.* **54**, 2680 (1989).

<sup>9</sup>N. Samarth, H. Luo, J. K. Furdyna, S. B. Qadri, Y. R. Lee, A. K. Ramdas, and N. Otsuka (unpublished).

<sup>10</sup>Y. R. Lee, Ph.D. thesis, Purdue University, 1987.

<sup>11</sup>Y. R. Lee, A. K. Ramdas, and R. L. Aggarwal, *Phys. Rev. B* **38**, 10 600 (1988).

<sup>12</sup>R. B. Bylisma, W. M. Becker, J. Kossut, U. Debska, and D. Yoder-Short, *Phys. Rev. B* **33**, 8207 (1986).

<sup>13</sup>See Table VII in the article by W. M. Becker, in *Diluted Magnetic Semiconductors* (Ref. 3), p. 35.

<sup>14</sup>M. M. Moriwaki, W. M. Becker, W. Gebhardt, and R. R. Galazka, *Phys. Rev. B* **26**, 3165 (1982).

<sup>15</sup>J. F. Mackay, W. M. Becker, J. Spałek, L. A. Kolodziejcki, R. L. Gunshor, and J. W. Richardson (unpublished).

<sup>16</sup>C. C. Klick and J. H. Schulman, in *Solid State Physics*, edited by F. Seitz and D. Turnbull (Academic, New York, 1957),

Vol. 5, p. 97.

<sup>17</sup>E.-K. Suh, A. K. Arora, A. K. Ramdas, and S. Rodriguez (unpublished).

<sup>18</sup>D. L. Peterson, D. U. Bartholomew, U. Debska, A. K. Ramdas, and S. Rodriguez, *Phys. Rev. B* **32**, 323 (1985).

<sup>19</sup>R. L. Aggarwal, S. N. Jaspersen, J. Stankiewicz, Y. Shapira, S. Foner, B. Khazai, and A. Wold, *Phys. Rev. B* **28**, 6907 (1983).

<sup>20</sup>A similar comparison was presented in our previous work (see Ref. 7), where the  $g$  factor of  $\text{Cd}_{0.84}\text{Mn}_{0.16}\text{Se}$  at  $T=5$  K was estimated from Ref. 19 to be  $g_{\text{hex}} \sim 200$  by interpolating between the  $x=0.1$  and 0.3 results. Such an interpolation did not take into account the antiferromagnetic interaction in the  $x$  dependence of the magnetization; when this is considered, we obtain a corrected value of  $g_{\text{hex}} \sim 288$ .

<sup>21</sup>D. L. Peterson, A. Petrou, W. Giriat, A. K. Ramdas, and S. Rodriguez, *Phys. Rev. B* **33**, 1160 (1986).

<sup>22</sup>L. Genzel, T. P. Martin, and C. H. Perry, *Phys. Status Solidi B* **62**, 83 (1974).

<sup>23</sup>The resultant MREI model force constants of  $\text{Cd}_{1-x}\text{Mn}_x\text{Se}$  are  $F_{\text{Cd-Se}}=2.44$ ,  $F_{\text{Mn-Se}}=2.02$ , and  $F_{\text{Cd-Mn}}=1.45$  in [ $10^6$  amu ( $\text{cm}^{-1}$ )<sup>2</sup>]. See Table II in Ref. 7 for the earlier values.

<sup>24</sup>A. V. Komarov, S. M. Ryabchenko, Yu. G. Semenov, B. D. Shanina, and N. I. Vitrikhovskii, *Zh. Eksp. Teor. Fiz.* **79**, 1554 (1980) [*Sov. Phys.—JETP* **52**, 783 (1980)].

<sup>25</sup>M. Nawrocki and R. R. Galazka, cited as Ref. 28 by J. A. Gaj, in *Proceedings of the 15th International Conference on the Physics of Semiconductors*, edited by S. Tanaka and Y. Toyozawa [*J. Phys. Soc. Jpn. Suppl. A* **49**, 797 (1980)].

<sup>26</sup>Bartholomew *et al.*, Ref. 2(b).

<sup>27</sup>M. M. Moriwaki, R. Y. Tao, R. R. Galazka, W. M. Becker, and J. W. Richardson, *Physica B* **117&118**, 467 (1983).

<sup>28</sup>J. E. Morales, W. M. Becker, and U. Debska, *Phys. Rev. B* **32**, 5202 (1985).

<sup>29</sup>J. E. Morales, W. M. Becker, B. I. Wang, U. Debska, and J. W. Richardson, *Phys. Rev. B* **40**, 1186 (1989).